Rate of energy absorption for a driven chaotic cavity

Alex Barnett^a, Doron Cohen^a and Eric J. Heller^{a,b}

^{a} Department of Physics, Harvard University;
^{b} Department of Chemistry and Chemical Biology, Harvard University;
Cambridge, MA 02138, USA

Abstract. We consider the response of a chaotic cavity in d dimensions to periodic driving. We are motivated by older studies of one-body dissipation in nuclei, and also by anticipated mesoscopic applications. For calculating the rate of energy absorption due to time-dependent deformation of the confining potential, we introduce an improved version of the wall formula. Our formulation takes into account that a special class of deformations causes no heating in the zero-frequency limit. We also derive a mesoscopic version of the Drude formula, and explain that it can be regarded as a special example of our calculations. Specifically we consider a quantum dot driven by electro-motive force which is induced by a time-dependent homogeneous magnetic field.

1. Introduction

The dynamics of a particle inside a cavity (billiard) in $d = 2$ or 3 dimensions is major theme in studies of classical and quantum chaos. Whereas the physics of time independent chaotic systems is extensively explored, less is known about the physics of time-dependent chaotic systems. The main exceptions are the studies of the kicked rotator and related systems [1]. However, the rotator (with no kicks) is a 1D integrable system, whereas we are interested in chaotic (2D or 3D) cavities.

Driven cavities were of special interest in the studies of one-body dissipation in nuclei [2, 3, 4, 5]. A renewed interest in this problem is anticipated in the field of mesoscopic physics. Quantum dots can be regarded as small 2D cavities whose shape is controlled by electrical gates. Another variation is driving a quantum dot by time-dependent magnetic field. In Section 6 we will explain that the calculation of the system response in the latter case can be regarded as a special example of the study in this paper. A similar observation applies to the case of a quantum dot driven by a homogeneous time-dependent electric field. However, in the latter case it is essential to take screening into account [6], and therefore our calculations no longer apply.

We consider a system of non-interacting particles inside a cavity whose walls can be deformed. We define a single parameter x that controls this deformation. We would like to consider the case where $x(t) = A \sin(\Omega t)$ is being changed periodically in time, where A is the amplitude and Ω is the driving frequency. In particular we are interested in the small frequency limit, meaning $\Omega \ll 1/\tau_{\text{col}}$. Here τ_{col} is the typical time between collisions with the moving walls of the cavity.

We will be interested in general deformations which need not preserve the billiard shape nor its volume. We can specify any deformation by a function $D(\mathbf{s})$, where $\mathbf{s}$ specifies the location of a wall element on the boundary (surface) of the cavity, and

$D(\mathbf{s})\delta x$ is the normal displacement of this wall element. There is a restricted class of deformations that are shape-preserving: they involve translations, rotations and dilations of the cavity. We will see that this class has special properties. Note that translations and rotations are also volume-preserving, in which case the associated time-dependent deformations can be described as 'shaking' the cavity.

What is the rate in which the 'gas' inside the cavity is heated up? The answer depends on the shape of the cavity, the deformation $D(\mathbf{s})$ involved, as well as on the amplitude A and the driving frequency Ω. Also the number of particles N and their energy distribution $\rho(E)$ should be specified.

For non-interacting particles the solution of this problem is reduced to the analysis of one-particle physics. This observation is self-evident for non-interacting classical particles, but it is also true for non-interacting fermions (see Appendix A). We would like to work within the framework of linear response theory (LRT). In such case one can write

$$\frac{d}{dt}\langle\mathcal{H}\rangle = \mu(\Omega) \times \tfrac{1}{2}(A\Omega)^2 \tag{1}$$

where the dissipation coefficient $\mu(\Omega)$ is amplitude independent. The small-Ω version of this formula can be written as

$$\frac{d}{dt}\langle\mathcal{H}\rangle = \mu V^2 \tag{2}$$

where $\mu = \mu(\Omega \to 0)$ is known as the friction coefficient, and $V = A\Omega/\sqrt{2}$ is the average root-mean-square (RMS) deformation velocity. For convenience let us define x as having units of length, such that V characterizes the velocity of the moving walls.

A necessary classical condition for the validity of LRT is $V \ll v_{\mathrm{E}}$ where $v_{\mathrm{E}} \equiv (2E/m)^{1/2}$ is the velocity of the particle [7, 8]. We also assume that the motion of the particle inside the cavity is globally chaotic, meaning no mixed phase space [10]. The criteria for having such a cavity are discussed in [11, 12]. The justification of LRT in the quantum-mechanical case is more subtle [8, 13, 14], and does not constitute a theme in this paper, although we do connect with the quantum case in Section 3. The theory to be presented assumes that LRT is a valid formulation of the problem.

As explained in Appendix A, LRT implies that the dissipation coefficient $\mu(\Omega)$ is related via a fluctuation-dissipation (FD) relation to a spectral function $\tilde{C}_{\mathrm{E}}(\Omega)$. Namely,

$$\mu(\Omega) = \frac{1}{2}\int_0^\infty \rho(E)dE \, \frac{1}{g(E)}\frac{\partial}{\partial E}\left[g(E)\tilde{C}_{\mathrm{E}}(\Omega)\right] \tag{3}$$

Here $\rho(E)$ is the energy distribution of the particles, and $g(E)$ is the density of states. The function $\tilde{C}_{\mathrm{E}}(\omega)$ is the noise power spectrum of the generalized 'force' associated with the parameter x. This function is the main object of the present study, and its precise definition is in Section 2. We shall chiefly explore how $\tilde{C}_{\mathrm{E}}(\omega)$ depends on the type of deformation involved, but also discuss effects due to the cavity shape.

In particular we are interested in the small frequency limit where μ is related to the fluctuations intensity

$$\nu_{\mathrm{E}} = \tilde{C}_{\mathrm{E}}(0) = \int_{-\infty}^\infty C_{\mathrm{E}}(\tau)d\tau. \tag{4}$$

The simplest estimate for ν_{E}, which we are going to call 'white noise approximation' (WNA), leads (in case of a 3D cavity) to the well known 'wall formula' [2]

$$\mu_{\mathrm{E}} = \frac{N}{\mathsf{V}}mv_{\mathrm{E}}\oint D(\mathbf{s})^2 d\mathbf{s} \tag{5}$$

where the subscript E implies that we are considering a microcanonical ensemble $\rho(E)$, the number of particles is N, and the volume of the cavity is V. The above version of the wall formula has been derived for the purpose of calculating the so-called one-body dissipation rate in nuclei. The original derivation of this formula is based on a simplified kinetic picture [2]. For alternate derivations using the LRT approach see [3]. For the generalization to any dimension d using the LRT-FD strategy see [8] and further references therein.

Our main purpose is to introduce an improved version of the wall formula, and to analyze the frequency dependence of $\mu(\Omega)$. This will involve a demonstration [16] that for special types of deformations (namely dilations, translations and rotations) the small-Ω dissipation rate is remarkably different from the naive expectation. As an application, the mesoscopic version of Drude formula for the *conductance* of a quantum dot in a uniform time-dependent magnetic field reduces to the the calculation of $\tilde{C}_E(\omega)$ for one of these special deformations (namely rotation), and leads to (see Section 6)

$$\mu(\Omega) \sim \frac{N}{A}\left(\frac{e^2}{m}\tau_{\mathrm{col}}\right)\frac{1}{1+(\tau_{\mathrm{col}}\Omega)^2} \tag{6}$$

where A is the area of the dot.

For our improved wall formula, we show that it is essential to project out the special components of a general deformation, and only then to estimate ν_E using the WNA. If the assumption of strong chaos cannot be justified, further corrections are required due to correlations between successive bounces.

The effect of interaction between the particles is not discussed in this paper. If the mean free path for inter-particle collisions is large compared with the size of the cavity, then we expect that our analysis still applies. If the mean free path is much smaller, then we get into the hydrodynamic regime. In the latter case we have a drag effect, and the dissipation rate is determined by the viscosity of the gas via Stokes' law.

2. The model system

Consider a particle whose canonical coordinates are $(\mathbf{r}, \mathbf{p})$ moving inside a cavity. The Hamiltonian is

$$\mathcal{H}(\mathbf{r}, \mathbf{p}; x) = \mathbf{p}^2/2m + U(\mathbf{r} - x\mathbf{D}(\mathbf{r})) \tag{7}$$

where $U(\mathbf{r})$ is the confining potential. We have introduced a (unitless) deformation 'field' $\mathbf{D}(\mathbf{r})$, and x is the controlling parameter. In this paper we assume that $U(\mathbf{r}) = 0$ inside the cavity. The volume of the cavity is V. Outside the cavity the potential $U(\mathbf{r})$ becomes very large. To be specific, one may assume that the walls exert a normal force f, and we take the hard wall limit $f \to \infty$. With the above assumptions about $U(\mathbf{r})$ it is clear that the deformation is completely specified by the boundary function $D(\mathbf{s}) \equiv \hat{\mathbf{n}}(\mathbf{s}) \cdot \mathbf{D}(\mathbf{s})$, where $\hat{\mathbf{n}}(\mathbf{s})$ is an outwards unit normal vector at the boundary point $\mathbf{s}$.

Most of our numerical tests will refer to the 2D cavity illustrated in Fig. 1a. It is a generalized two-dimensional Sinai billiard formed from concave arcs of circles with two different radii. Typical parameters used are $a=2$, $b=1$, $\theta_1=0.2$, $\theta_2=0.5$, for which the average collision rate with the wall is $(1/\tau_{\mathrm{bl}}) \approx 0.63$. This billiard has been chosen because it has 'hard chaos': There is no mixed phase space, and there are no marginally-stable orbits (see Section 7). In Fig. 1b we show three example
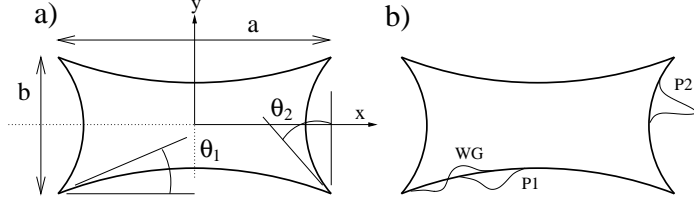
Figure 1. **a**) The generalized two-dimensional Sinai billiard which has been used for our numerical studies. **b**) Three example deformations are illustrated. Note that they are shown exaggerated in strength.

deformations. For illustration purposes we have selected three 'localized' deformations. See Tables 1 and 2 for a full list of deformations that have been tested in our numerical work.

Associated with the parameter x is the fluctuating quantity

$$\mathcal{F}(t) = -\left.\frac{\partial \mathcal{H}(\mathbf{r}, \mathbf{p}; x)}{\partial x}\right|_{x=0} \tag{8}$$

where the time-dependence arises from that of the trajectory $(\mathbf{r}(t), \mathbf{p}(t))$. This quantity can be thought of as the generalized time-dependent 'force' associated with the parameter x. For the Hamiltonian (7) we can write

$$\mathcal{F}(t) = \mathbf{D}(\mathbf{r}) \cdot \nabla U(\mathbf{r}) = -\mathbf{D}(\mathbf{r}) \cdot \dot{\mathbf{p}}. \tag{9}$$

Recognizing $\dot{\mathbf{p}}$ as the force on the gas particle, we see that $\mathcal{F}(t)$ is a train of spikes (see Fig. 2a). Namely, the fluctuating force $\mathcal{F}(t)$ consists of impulses whose maximum duration is $\tau_0 = 2mv_{\mathrm{E}}/f$. In the hard wall limit $\tau_0 \to 0$, and we can write

$$\mathcal{F}(t) = \sum_i 2mv_{\mathrm{E}} \, \cos(\theta_i) \, D_i \, \delta(t - t_i) \tag{10}$$

where i labels collisions: t_i is the time of a collision, D_i stands for $D(\mathbf{s}_i)$ at the location $\mathbf{s}_i$ of a collision, and $v_{\mathrm{E}}\cos(\theta_i)$ is the normal component of the particle's collision velocity. The above sequence of impulses is characterized by an average rate of collisions $1/\tau_{\mathrm{col}}$. The quantitative definition of τ_{col} is postpone to Section 4. Note however that τ_{col} may be much larger that the ballistic time τ_{bl}. The ballistic time is the average time between collisions with the boundary. We have $\tau_{\mathrm{col}} \gg \tau_{\mathrm{bl}}$ whenever a deformation involves only a small piece of the boundary. Finally we note that if the deformation is volume-preserving then $\langle \mathcal{F}(t) \rangle = 0$. Otherwise it is convenient to subtract the (constant) average value $F(x)$ from the above definition of $\mathcal{F}(t)$. This convention is reflected in our illustration (Fig.2a).

We define the auto-correlation function of $\mathcal{F}(t)$ as follows:

$$C_{\mathrm{E}}(\tau) \equiv \langle \mathcal{F}(t)\mathcal{F}(t+\tau) \rangle_{\mathrm{E}} \tag{11}$$

The subscript $_{\mathrm{E}}$, whenever used, suggests that the average over initial conditions is of microcanonical type, with energy E. Note that $C_{\mathrm{E}}(\tau)$ is defined using the time independent ('frozen') Hamiltonian, and therefore is independent of t. The auto-correlation function $C_{\mathrm{E}}(\tau)$ can be handled as a time-average rather than an ensemble-average (by ergodicity). The resulting construction is illustrated in Fig. 2b, where we illustrate the projection of $\mathcal{F}(t_1)\mathcal{F}(t_2)$ onto the $\tau \equiv t_2 - t_1$ axis. The contribution for the self correlation is shaded. The forms of the resultant $C_{\mathrm{E}}(\tau)$ and its Fourier

transform $\tilde{C}_{\mathrm{E}}(\omega) \equiv \int C_{\mathrm{E}}(\tau)\exp(i\omega\tau)d\tau$ are illustrated schematically in Figs. 2c and 2d. Note that the $\omega \to 0$ limit of $\tilde{C}(\omega)$ is equal to the area under $C(\tau)$.

The auto-correlation function $C_{\mathrm{E}}(\tau)$ consists of a $\tau = 0$ ('self') peak due to the self-correlation of the spikes, and of an additional smooth ('non-self') component due to correlations between successive bounces. This implies [9] that pronounced correlations are usually characterized by the time scale τ_{bl}, rather than τ_{col}. Consequently the associated frequency scale for non-universal structures is $\omega \sim 1/\tau_{\mathrm{bl}}$. Another relevant time scale is the ergodic time t_{erg} which is the inverse of the average Lyapunov (instability) exponent. Beyond t_{erg} the correlations become vanishingly small. Non-negligible tails may arise only if the motion has marginally stable orbits.

As explained in the Introduction, we shall be most interested in the noise intensity ν_{E} defined by (4). Observing that $\mathcal{F}(t)$ is linear in $D(\mathbf{s})$, it follows that the noise intensity is a quadratic functional

$$\nu_{\mathrm{E}} = \oint\oint d\mathbf{s}_1 d\mathbf{s}_2 \, D(\mathbf{s}_1)\gamma_{\mathrm{E}}(\mathbf{s}_1,\mathbf{s}_2)D(\mathbf{s}_2), \tag{12}$$

where the kernel γ_{E} depends on both the cavity shape and the particle energy E [3]. Furthermore, billiards are *scaling systems* in the sense that a change in E leaves the trajectories unchanged. From this and (10) we have the scaling relation $\gamma_{\mathrm{E}}(\mathbf{s}_1,\mathbf{s}_2) = m^2 v_{\mathrm{E}}^3 \cdot \hat{\gamma}(\mathbf{s}_1,\mathbf{s}_2)$, where the scaled kernel depends entirely on the geometrical shape of the cavity. However, the reason for being interested in *approximations* for ν_{E} is that the exact result for the kernel $\hat{\gamma}$ is very complicated to evaluate, and involves a sum over all classical paths from $\mathbf{s}_1$ to $\mathbf{s}_2$ (see [3]).

3. Quantum-classical correspondence

This paper applies classical physics in order to analyze the response of a wide class of systems, including mesoscopic systems where quantum mechanics may play a role. How much of a compromise is a classical analysis of the dissipation? This question has been addressed in [13, 8]. In the level of one-particle physics the answer is as follows: within the framework of LRT the only difference between the classical formulation and the quantal one is involved in replacing the classical definition of $C_{\mathrm{E}}(\tau)$ by the corresponding quantum-mechanical definition. In the level of many (non-interacting) particles the only further modification is associated with the application of the FD relation, as discussed in Appendix A (See Eq.(A.6)). We would like to re-emphasize that we assume in this paper that we are in an (A,Ω) regime where LRT is a valid formulation. The quantum adiabatic regime (extremely small Ω), and the non-perturbative regime (see discussion in [14]) are excluded from our considerations.

Thus the only remaining question is whether a classical calculation of $\tilde{C}_{\mathrm{E}}(\omega)$ is a good approximation quantum-mechanically. The answer is that the quantum-classical correspondence here is remarkable. It has been tested for a few example systems [16, 17, 18]. In Fig. 3 we demonstrate correspondence for the stadium billiard for three types of deformations: DI (dilation), W2 (periodic oscillation around the perimeter), and P (wide 'piston' existing only on the top edge). The RMS estimation error is 3% for the classical calculation and 10% for the quantum calculation. The quantum estimate of $\tilde{C}_{\mathrm{E}}(\omega)$ amounts to computing boundary overlap integrals of the eigenfunctions (see [16]). We have used all 451 states lying between wavenumbers $398 < k < 402$, where the mean level spacing is $\Delta \approx 8.8 \times 10^{-3}$ in ω units. Note that there are $\sim 10^2$ de Broglie wavelengths across the system. The stadium was
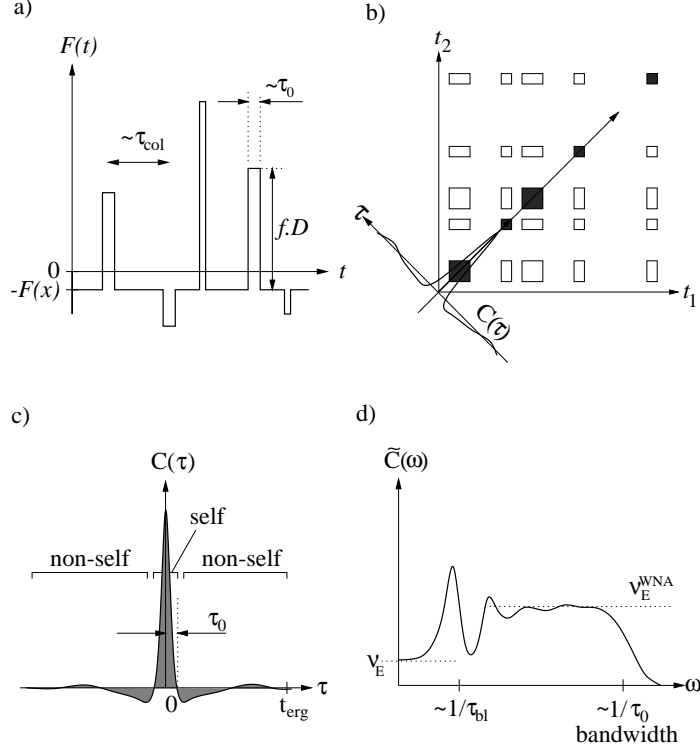
Figure 2. The fluctuating force $\mathcal{F}(t)$ looks like a train of impulses (**a**). Due to ergodicity the autocorrelation function $C(\tau)$ can be regarded as a time average (**b**). The resultant autocorrelation function (**c**) and the associated power spectrum (**d**) may be characterized by non universal features. See text for further explanations.

chosen because it enables efficient quantization using the method of Vergini and Saraceno [19, 20]. An especially good basis set is known for this shape [21].

4. The white noise approximation

The most naive estimate of the fluctuations intensity is based on the WNA. Namely, one assumes that the correlation between bounces can be neglected. This corresponds [3] to the *local* part of the kernel (12). In such case only the self-correlation of the spikes is taken into consideration and one obtains [8]

$$\nu_{\text{E}} \approx (2mv_{\text{E}})^2 \left\langle \sum_i \cos^2(\theta_i) \ D_i^2 \ \delta(t - t_i) \right\rangle_{\text{E}} \tag{13}$$

and from here (see [8]) using ergodicity,

$$\nu_{\text{E}} \approx 2m^2 v_{\text{E}}^3 \langle |\cos\theta|^3\rangle \frac{1}{V} \oint [D(\mathbf{s})]^2 d\mathbf{s} \tag{14}$$

where the geometric factor for $d = 2, 3, \cdots$ is $\langle |\cos(\theta)|^3\rangle = 4/(3\pi), 1/4, \cdots$. If we can use the convention $|D(\mathbf{s})| \sim 1$ over the deformed region (and zero otherwise), then we can write the WNA as $\nu_{\text{E}} = (2mv_{\text{E}})^2 \times (1/\tau_{\text{col}})$ where $(1/\tau_{\text{col}})$ defines the effective collision rate. For a more careful discussion see Appendix F of Ref.[8]. Note again
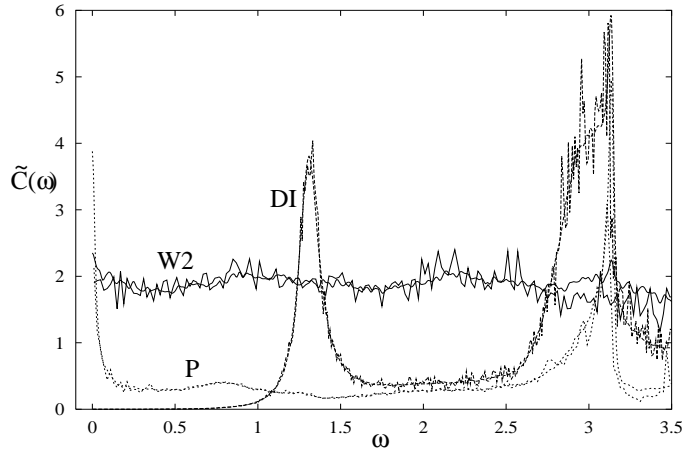
Figure 3. Agreement between quantum and classical $\tilde{C}_{\mathrm{E}}(\omega)$ in the two-dimensional quarter-stadium billiard for three example deformations (see text). In each case classical is shown as a thick line, and quantum a thin line. The y-axis has been displaced to clearly show the $\omega \to 0$ behavior. The singular peak at $\omega = \pi$ is due to the 'bouncing ball' orbit.

that τ_{col} can be much larger than the ballistic time τ_{bl} in the case that only a small piece of the boundary is being deformed.

The use of the WNA can be justified whenever successive collisions are effectively uncorrelated. The applicability of such an assumption depends on the shape of the cavity (which will determine the decay of correlations via the typical Lyapunov exponent) as well as on the type of deformation involved. If we have the cavity of Fig. 1a, and the deformation involves only a small piece of the boundary (*e.g.* see Fig. 1b), then successive collisions with the *deformed part* of the boundary are effectively uncorrelated. This is so because there are many collisions with static pieces of the boundary before the next effective collision (with non zero D_i) takes place. If the deformation involves a large piece (or all) of the boundary, we can still argue that successive collisions are effectively uncorrelated provided $D(\mathbf{s})$ is 'oscillatory' enough (ie changes sign many times along the boundary). These expectations are qualitatively confirmed by the numerical results of Fig. 4. Here we show a sequence of deformation types for which the WNA performs increasingly well: FR (for which sensitivity to the vertical least-unstable periodic orbit causes large correlation effects and large deviations from WNA), W8 (oscillatory deformation changes sign many times around the perimeter, giving better agreement with WNA), P1 (localized 'piston' type deformation, for which WNA is good), and DF (random function of zero correlation-length along the perimeter, showing complete WNA agreement).

The numerical evaluation of $\tilde{C}_{\mathrm{E}}(\omega)$ throughout this work is performed by squaring the Fourier transform of a single long sample of $\mathcal{F}(t)$ ($\sim 10^6$ consecutive collisions). Ergodicity ensures that the properties of a single trajectory reproduce the desired ensemble-average $\langle \cdots \rangle_{\mathrm{E}}$. In practice the power spectrum of a single sample is a stochastic quantity with no correlations in ω-space. To estimate the underlying noise spectrum $\tilde{C}_{\mathrm{E}}(\omega)$ a smoothing convolution in ω-space is performed. In the figures a smoothing width of 10^{-2} is typical, giving 3% RMS estimation error. The δ-function nature of $\mathcal{F}(t)$ is handled by convolving in the time-domain with a suitably-narrow
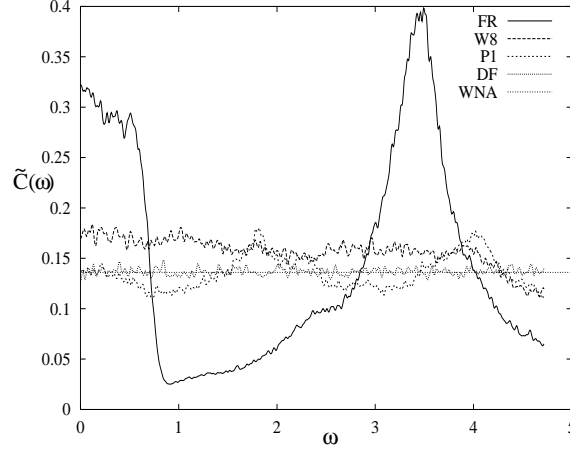
Figure 4. The white-noise approximation estimate (WNA is the horizontal dotted line) compared to actual $\tilde{C}_E(\omega)$ power spectra for some example deformations of the 2D generalized Sinai billiard, with $m = v = 1$. (The RMS estimation error of 3% can be seen as multiplicative noise with short correlation length in ω). Deformation functions are defined in Table I, and discussed further in the text.

key	description	surface deformation function $D(s)$
CO	constant	1
Wn	n periods	$\cos(2\pi n s/L)$
DF	diffuse	random[-1,1] (equivalent to W∞)
FR	fracture	$\mathrm{sgn}(x(s))$ if on top or bottom, else 0
SX	shift-x	$\mathrm{sgn}(x(s))$ if on left or right, else 0
P1	piston 1	$10\exp(-\frac{1}{2}\alpha^2)$, $\alpha=(s/L-0.3)/0.01$
P2	piston 2	$10\exp(-\frac{1}{2}\alpha^2)$, $\alpha=(s/L-0.6)/0.005$
WG	wiggle	$5\alpha\exp(-\frac{1}{2}\alpha^2)$, $\alpha=(s/L-0.25)/0.02$

Table 1. Key to deformation types used for numerical 2D billiard experiments in this paper. L is the billiard perimeter. The deformation is described by a function $D(s)$, where s is measured counter-clockwise along the perimeter with $s = 0$ at the upper left corner. In the 'fracture' and 'shift-x' cases we use the horizontal Cartesian coordinate $x(s)$.

Gaussian. This enables the signal to be sampled uniformly in time, and hence we can benefit from use of the Fast Fourier Transform procedure.

It might be asked whether the exponential growth in sensitivity to numerical round-off error invalidates the computation of the properties of a long classical trajectory. The answer is no: it has been shown that in simple two-dimensional chaotic maps such as ours, a numerically-generated 'pseudo-trajectory' *shadows* (is very close to) a true trajectory with slightly different initial conditions [22]. However, as we shall see, the differences in $\omega \to 0$ behavior (in the hard chaos case) do not in fact rely on correlation properties over times any longer than t_{erg}.
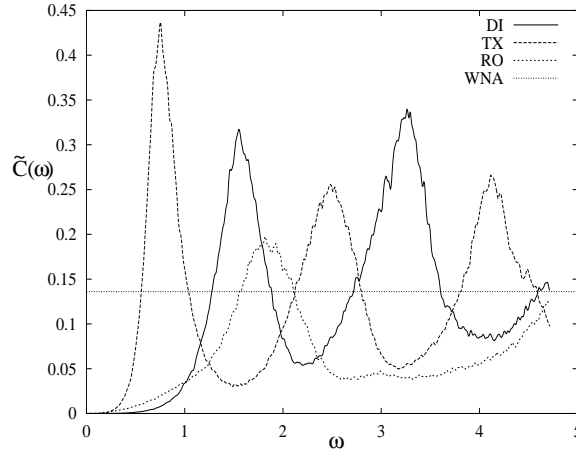
Figure 5. The WNA estimate compared to actual $\tilde{C}(\omega)$ noise power spectra for example 'special' deformation types: DI (dilation), TX (translation) and RO (rotation). See Table II for definitions. The WNA fails to predict the vanishing in the small ω limit.

key	description	deformation field
DI	dilation about origin	$\mathbf{D}(\mathbf{r}) = \mathbf{r}$
TX	x-translation	$\mathbf{D}(\mathbf{r}) = \mathbf{e}_x$
TY	y-translation	$\mathbf{D}(\mathbf{r}) = \mathbf{e}_y$
RO	rotation about origin	$\mathbf{D}(\mathbf{r}) = \mathbf{e}_z \times \mathbf{r}$

Table 2. Key to the four 'special' deformations in 2D. The unit vectors $\mathbf{e}_x$ and $\mathbf{e}_y$ are in the plane (see Fig. 1), and $\mathbf{e}_z$ is in the perpendicular direction. In the case of dilation and rotation $\mathbf{D}$ could be made unitless by dividing by a constant length.

5. 'Special' deformations

The WNA dramatically fails (see Fig. 5) for dilation, translations and rotations (see Table 5 for their definitions in 2D). It is not surprising that the WNA is 'bad' for these deformations because their $D(\mathbf{s})$ are slowly-changing delocalized functions of s. However, what is remarkable is that $\tilde{C}_{\mathrm{E}}(\omega)$ for this type of deformations *vanishes* in the limit $\omega \to 0$. Such deformations we would like to call 'special' [16]. More generally, we would like to say that a deformation is 'special' if the associated fluctuation intensity is $\nu_{\mathrm{E}} = 0$.

A result that follows from the considerations of Appendix B is that a linear combination of special deformation is also special. Therefore the special deformations constitute a linear space of functions. We believe that this linear space is spanned by the following basis functions: one dilation, d translations, and $d(d-1)/2$ rotations. However we are not able to give a rigorous mathematical argument that excludes the possibility of having a larger linear space. In other words, we believe that any special deformation can be written as a linear combination of dilation, translations and rotations.

We will explain the observed $\nu_{\mathrm{E}} = 0$, starting with the case of translations and dilations. For translations we have $\mathbf{D} = \mathbf{e}$, where $\mathbf{e}$ is a constant vector that defines a

direction in space. We can write $\mathcal{F}(t) = (d/dt)^2 \mathcal{G}(t)$ where $\mathcal{G}(t) = -m\mathbf{e} \cdot \mathbf{r}$. A similar relation holds for dilation $\mathbf{D} = \mathbf{r}$ with $\mathcal{G}(t) = -\frac{1}{2}m\mathbf{r}^2$. It follows that $\tilde{C}(\omega) = \omega^4 \tilde{C}_G(\omega)$, where $\tilde{C}_G(\omega)$ is the power spectrum of $\mathcal{G}(t)$. If $\tilde{C}_G(\omega)$ is a bounded function (as it must be when correlations are short-range), it immediately follows that $\tilde{C}(0) = 0$. Moreover since $\mathcal{G}(t)$ is a simple function of the particle position, we can assume it is a fluctuating quantity that looks like white noise on timescales $> t_{\mathrm{erg}}$. It follows that $\tilde{C}(\omega)$ is generically characterized by ω^4 behavior for either translations or dilations.

We now turn to consider the case of rotations. This case is of particular interest because of its relation to the Drude conductance calculation in a uniform driving magnetic field (see the following section). For rotations we have $\mathbf{D} = \mathbf{e} \times \mathbf{r}$, and we can write $\mathcal{F}(t) = (d/dt)\mathcal{G}(t)$, where $\mathcal{G}(t) = -\mathbf{e} \cdot (\mathbf{r} \times \mathbf{p})$, is a projection of the particle's angular momentum vector [15]. Consequently $\tilde{C}(\omega) = \omega^2 \tilde{C}_G(\omega)$. Assuming the angular momentum is a fluctuating quantity that looks like white noise on timescales $> t_{\mathrm{erg}}$, it follows that $\tilde{C}(\omega)$ is generically characterized by ω^2 behavior.

Thus we have predictions for the power-laws in the regime $\omega < 1/t_{\mathrm{erg}}$ for special deformations (assuming hard chaos). These have been verified numerically in our previous work [16], with a special emphasis on the case of dilation. The case of dilation plays a vital role in a highly-successful numerical billiard diagonalization method that has been introduced recently [19].

For special deformations we have $\tilde{C}(\omega) = 0$ in the limit $\omega = 0$, and consequently the dissipation coefficient vanishes ($\mu = 0$). It should be noted that for the case of a general combination of translations and rotations this result follows from a simpler argument. Taking $\Omega \to 0$ while keeping $A\Omega$ constant corresponds to constant deformation velocity ($\dot{x} = $const). Transforming the time-dependent Hamiltonian into the reference frame of the cavity (which is uniformly translating or rotating with constant velocity) gives a *time-independent* Hamiltonian. In the new reference frame the energy is a constant of the motion, which implies that the system cannot absorb energy (no dissipation effect), and hence we must indeed have $\mu = 0$.

6. Drude mesoscopic conductance for 2D dot

Consider a 2D quantum dot in a homogeneous (perpendicular) magnetic field (see Fig. 6b). The one-particle Hamiltonian is

$$\mathcal{H}(\mathbf{r}, \mathbf{p}; \Phi(t)) = \frac{1}{2m}\left[\mathbf{p} - e\mathbf{A}(\mathbf{r}; \Phi(t))\right]^2 + U(\mathbf{r}) \tag{15}$$

The dot is defined by the confining potential $U(\mathbf{r})$, and we choose the magnetic field as the controlling (driving) parameter. Periodic driving means $\Phi(t) = A\sin(\Omega t)$. The vector potential is given by

$$\mathbf{A}(\mathbf{r}; \Phi) = \frac{1}{2}\left(\frac{\Phi}{\mathsf{A}}\hat{\mathbf{z}}\right) \times \mathbf{r} \tag{16}$$

where A is the area of the dot, Φ/A is the magnetic field, and $\hat{\mathbf{z}}$ is its (perpendicular) direction.

Referring to Eq.(2) one should realize that by Faraday's law $V = \dot{\Phi}$ is the induced electromotive force (measured in volts). Hence μ is just the conductance. The fluctuating quantity that is associated with Φ has the meaning of electric current:

$$\mathcal{I}(t) = -\frac{\partial \mathcal{H}}{\partial \Phi} = \frac{e}{2\mathsf{A}}(\hat{\mathbf{z}} \times \mathbf{r}) \cdot \mathbf{v} \tag{17}$$

In the conventional ring geometry (Fig. 6a) the current is just $\mathcal{I}(t) = (e/\mathsf{L})v$, where L is the perimeter, and v is the tangential velocity. In the general cavity case (Fig. 6b) $\mathcal{I}(t)$ can be thought of as the angular momentum of the charge.

The Drude mesoscopic conductance is given by the frequency-dependent version of the FD relation Eq.(A.6). With one-particle density of states corresponding to 2D gas Eq.(A.6) becomes

$$\mu(\Omega) = \frac{N}{mv_{\mathrm{F}}^2}\tilde{C}_{\mathcal{I}}(\Omega) \tag{18}$$

where the Fermi velocity is related to the Fermi energy $E_{\mathrm{F}} = \frac{1}{2}mv_{\mathrm{F}}^2$. The power spectrum of the electric current $\tilde{C}_{\mathcal{I}}(\omega)$ is the Fourier transform of the current-current correlation function. In standard derivations of the Drude formula it is assumed that this correlation function is exponential:

$$C_{\mathcal{I}}(\tau) \quad \sim \quad \frac{e^2}{\mathsf{A}}v_{\mathrm{F}}^2 \ \exp\left(-\frac{|\tau|}{\tau_{\mathrm{col}}}\right) \tag{19}$$

leading to the Lorentzian Eq.(6). However, for a given dot shape $C_{\mathcal{I}}(\tau)$ is not really an exponential, but rather reflects the system-specific geometry. Below we discuss two limits in which we can obtain approximations for $C_{\mathcal{I}}(\tau)$ and hence (via Eq.(18)) for the frequency-dependent conductance $\mu(\Omega)$.

The current $\mathcal{I}(t)$ is a piecewise constant function of time. It is constant between collisions with the walls because of conservation of angular momentum. The derivative of this quantity, $\mathcal{F}(t) = \dot{\mathcal{I}}$, is a train of spikes. It formally coincides (using (9)) with the $\mathcal{F}(t)$ of the deformation $\mathbf{D}(\mathbf{r}) = (e/(2m\mathsf{A}))\hat{\mathbf{z}} \times \mathbf{r}$, corresponding to rotation around the z axis. It follows that the current-current correlation $C_{\mathcal{I}}(\tau)$ is trivially related to the $\mathcal{F}(t)$ correlation function $C(\tau)$ as follows:

$$\tilde{C}_{\mathcal{I}}(\omega) \ = \ \frac{1}{\omega^2}\tilde{C}(\omega) \tag{20}$$

Thus we see that the calculation of 'conductance' is formally equivalent to a special case of deformation, namely a rotation.

There are two limits in which we can get approximation for $\tilde{C}_{\mathcal{I}}(\omega)$. For small frequencies $\omega \ll (1/\tau_{\mathrm{col}})$ we may use the following simple estimate:

$$\tilde{C}_{\mathcal{I}}(\omega) \ = \ \langle \mathcal{I}^2 \rangle \times 2\tau_{\mathrm{col}} \ = \ \frac{1}{4}e^2\frac{\langle \mathbf{r}^2 \rangle}{\mathsf{A}^2} \ v_{\mathrm{F}}^2 \times \tau_{\mathrm{col}} \tag{21}$$

The first equality can be taken as an operative definition of the correlation time τ_{col} in the context of this calculation. Obviously, up to a system-specific geometrical factor this result ($\sim \omega^0$) agrees with the standard Drude result. For ring geometry one should make the replacements $\langle \mathbf{r}^2 \rangle \mapsto (\mathsf{L}/(2\pi))^2$ and $\mathsf{A} \mapsto \pi(\mathsf{L}/(2\pi))^2$ where L is the length of the wire (perimeter of the ring). Thus one obtains $\tilde{C}_{\mathcal{I}}(\omega) = ((e/\mathsf{L})v_{\mathrm{F}})^2$ leading to the standard-looking Drude formula for a mesoscopic wire $\mu = (N/\mathsf{L}^2) \times (e^2/m) \times \tau_{\mathrm{col}}$.

In the limit $\omega \gg (1/\tau_{\mathrm{col}})$ we can get a much more satisfying result. The fluctuating quantity $\mathcal{F}(t) = \dot{\mathcal{I}}(t)$ is the same as (9) with $\mathbf{D}(\mathbf{r}) = (e/(2m\mathsf{A}))\hat{\mathbf{z}} \times \mathbf{r}$, corresponding to rotation. Using the WNA of Eq.(14), and dividing by ω^2 as in (20) we get

$$\tilde{C}_{\mathcal{I}}(\omega) = \left[\frac{2}{3\pi}\frac{e^2}{\mathsf{A}^3}v_{\mathrm{F}}^3 \oint |\mathbf{n} \times \mathbf{r}|^2 ds\right]\frac{1}{\omega^2} \tag{22}$$

Again, up to system-specific geometrical factor this result ($\sim \omega^{-2}$) agrees with the standard Drude result. The latter expression should become exact as we go to large
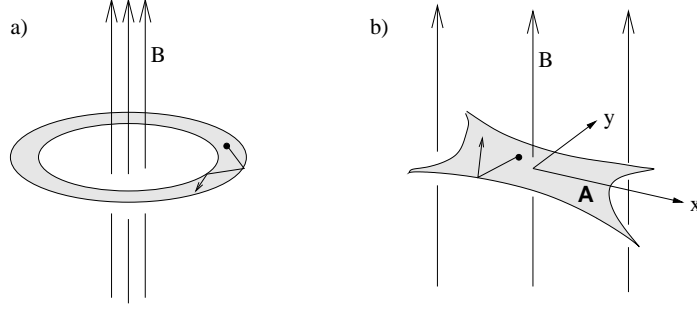
Figure 6. Two possible mesoscopic geometries which exhibit conductance when driven by a magnetic field: a) conventional ring of perimeter L enclosing the time-dependent flux, b) ballistic two-dimensional chaotic dot (cavity) of area A in a uniform time-dependent magnetic field.

frequencies, where the only significant contribution comes form the self-correlation of the $\mathcal{F}(t)$ spikes (see Fig. 2d).

Eq.(21) leads (via (18)) to the small frequency Drude result, while the WNA of Eq.(22) gives the Lorentzian tail of the Drude result. An exact result for the frequency-dependent conductance can be calculated numerically for a given geometrical shape. In Fig. 7 we display a plot of $\mu(\Omega) \propto \tilde{C}_{\mathcal{I}}(\Omega)$, which shows both the constant behavior at small Ω and the convergence to the large-Ω WNA approximation. System-specific features are expressed by the deviation from standard Lorentzian in the intermediate frequency regime.

Finally we consider driving a quantum dot with homogeneous electric field in the x direction, in which case the Hamiltonian contains the interaction term $-e\mathcal{E}(t)x$. For calculation of the response in such a case one should evaluate the dipole-dipole correlation function $C_{\mathcal{P}}(\tau)$ where $\mathcal{P}(t) = ex$. The latter is related to translations, where the deformation field is $\mathbf{D} = \hat{\mathbf{x}}$. Consequently we get $C_{\mathcal{P}}(\tau) = (1/\omega^4)C(\tau)$. However, this result is not of great interest, because the screening effect leads to modification of the effective one-particle Hamiltonian, such that the actual electric field inside a quantum dot is much smaller than the applied field.

7. The white noise assumption revisited

In Section 4 we have assumed that generic fluctuating quantities such as $\mathbf{r}^2$ and $\mathbf{e} \cdot \mathbf{r}$ and $\mathbf{e} \cdot (\mathbf{r} \times \mathbf{p})$ have a white noise power spectrum for $\omega \ll 1/\tau_{\mathrm{bl}}$. In section 8 we are going to suggest that this white noise assumption is approximately true for any fluctuating quantity $\mathcal{F}(t)$ that comes from a normal deformation (the term 'normal' will be defined there).

Obviously, the goodness of the 'white noise assumption' in the two cases mentioned is related to the chaoticity of the system, and should be tested for particular examples. This has been done so for the cavity of Fig. 1 (see [16], and Figs. 4 and 9). This cavity is an example of a 'scattering billiard' and so exhibits strong chaos [11]. If the motion is *not* strongly chaotic we may get a $C(\tau)$ that decays like a power law (say $1/\tau^{1-\gamma}$ with $0 < \gamma \le 1$) rather than an exponential [11, 23, 24, 25, 26]. In such case
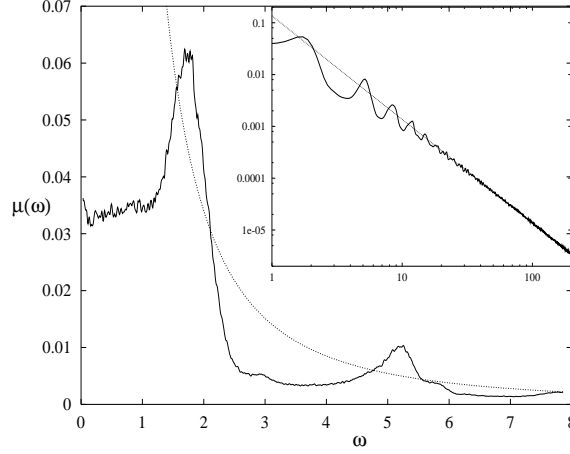
Figure 7. Calculation of dissipation coefficient $\mu(\Omega)$ (arbitrary units) for driving of a chaotic mesoscopic billiard system with a constant magnetic field at frequency Ω. The billiard chosen is the 2D generalized Sinai of Fig. 1a. The dotted line $\text{WNA}(\mathcal{F})$ is the high-frequency estimate assuming $\mathcal{F}(t) \equiv \dot{\mathcal{I}}$ is white noise. The convergence to this ω^{-2} result is clearly visible in the log-log inset plot.

the universal behavior is modified: we get $\omega^{-\gamma}$ behavior for $\tilde{C}_{\text{E}}(\omega)$ at small frequencies (ν_{E} diverges), signifying faster-than-diffusive energy spreading in Eq.(A.2) [26]. The stadium is an example where such a complication may arise: an ergodic trajectory can remain in the marginally-stable 'bouncing ball' orbit (between the top and bottom edges) for long times, with a probability scaling as t^{-1} [23, 24, 25]. Depending on the choice of $D(\mathbf{s})$ this *may* manifest itself in $C(\tau)$. For example, in Fig. 3 the deformation P involves a distortion confined to the upper edge, and the resulting sensitivity to the bouncing ball orbit leads to large enhancement of the fluctuations intensity $\tilde{C}(\omega{=}0)$, and is suggestive of singular behavior for small ω.

If the billiard has a mixed phase space (which is the generic case), then the integrable component does not contribute to diffusive energy spreading. Proposals have been made to account for this via a phase-space volume factor [10].

8. Decomposition of general deformations

The failure of the WNA for 'special' deformations also extends to the much wider class of deformations which are *similar* to special. This is demonstrated in Fig. 8. It should be emphasized that this failure happens even if the cavity is strongly chaotic.

We seek an analytical estimate for $\tilde{C}(\omega)$, and in particular for its zero-frequency limit ν. This estimate should apply to any (general) deformation, including the case of 'close-to-special' deformations. It would be useful to regard any general deformation as a combination of 'special' component and 'normal' component. The formulation of this idea is the theme of the present section. Supporting numerical evidence is gathered in the next section.

The special deformations (for which we have $\nu = 0$) constitute a linear space, meaning that any sum of special deformations is also a special one. Now we would like to conjecture that there is also a linear space of 'normal' deformations. By definition, for 'normal' deformation $\mathcal{F}(t)$ looks like an uncorrelated random sequence
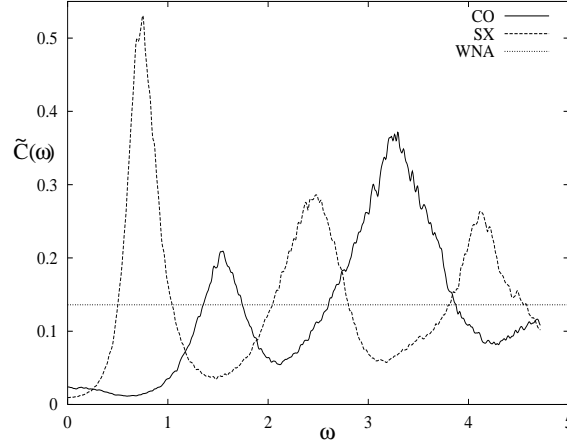
Figure 8. The failure of the WNA estimate for $\tilde{C}(\omega)$ for deformation types CO (similar to DI) and SX (similar to TX). The WNA is clearly a vast overestimate of the small-ω limit. See Tables I and II for explanation of deformation types.

of impulses, and consequently the WNA is a reasonable approximation. The notion of randomness can be better formulated as in Appendix C leading to Eq.(C.4). However in practice (C.4) is not useful, because it cannot be applied as an actual classification tool. (Eq.(C.4) is never satisfied exactly). Still we are going to demonstrate that there is a *unique* way to identify the subspace of normal deformations, if we insist on a maximal (*i.e.* the most inclusive) definition of this subspace.

It is important to clarify the heuristic reasoning of having linear space of normal deformations. The $\mathcal{F}(t)$ that corresponds to some normal deformation $D(\mathbf{s})$ looks like white noise. It means that only self-correlations of its spikes are statistically significant. If we have two such generic quantities, say $\mathcal{F}_1(t)$ and $\mathcal{F}_2(t)$, then we expect $\mathcal{F}_1(t) + \mathcal{F}_2(t)$ to share the same property.

The correlation function of $\mathcal{F}(t) = \mathcal{F}_1(t) + \mathcal{F}_2(t)$ can be written formally as

$$C_{1+2}(\tau) = C_1(\tau) + C_2(\tau) + 2C_{1,2}(\tau) \tag{23}$$

where $C_{1,2}(\tau)$ is the *cross-correlation function*. In Appendix B we argue the following

$$\int_{-\infty}^{\infty} C_{1,2}(\tau)d\tau = 0$$
$$\text{if 1=general, 2=special} \tag{24}$$

This result is exact, and does not involve any approximation. In Appendix C we argue the following

$$C_{1,2}(\tau) \approx c \times \left[\oint D_1(\mathbf{s})D_2(\mathbf{s})d\mathbf{s} \right] \delta(\tau)$$
$$\text{if 1=normal, 2=general} \tag{25}$$

where $c = 2m^2 v_{\mathrm{E}}^3 \langle |\cos\theta|^3 \rangle / \mathsf{V}$. This result is an approximation, which is expected to be as good as our assumption regarding the 'normality' of the deformation $D_1(\mathbf{s})$. Consider now the case where $D_1(\mathbf{s})$ is normal and $D_2(\mathbf{s})$ is special. Both Eq.(24) and Eq.(25) should apply. But these equations are consistent if and only if $D_1(\mathbf{s})$ is

orthogonal to $D_2(\mathbf{s})$. We say that $D_1(\mathbf{s})$ and $D_2(\mathbf{s})$ are orthogonal ($1 \perp 2$) using the following definition:

$$\text{orthogonality} \quad \Leftrightarrow \quad \oint D_1(\mathbf{s})D_2(\mathbf{s})d\mathbf{s} = 0 \qquad (26)$$

Thus we have proved that normal deformations must be orthogonal (in the sense of (26)) to special deformations. Obviously we have proved here a necessary rather than a sufficient condition for 'normality'. However, if we insist on a maximal definition for the subspace of normal deformations, then we get a unique identification. Namely, a deformation is classified as 'normal' if it is orthogonal to the subspace of special deformations.

The practical consequences of Eq.(24) and Eq.(25) are as follows:

$$\nu_{1+2} = \nu_1 \quad \text{if } 1\text{=general, } 2\text{=special} \qquad (27)$$

and

$$\nu_{1+2} \approx \nu_1 + \nu_2 + 2c \oint D_1(\mathbf{s})D_2(\mathbf{s})d\mathbf{s}$$

$$\text{if } 1\text{=normal, } 2\text{=general} \qquad (28)$$

These results are tested in the next section.

9. Addition of deformations: numerical tests

On the basis of the discussion in the previous section we *define* normal deformation as those that are orthogonal to all special deformations, in the sense of Eq. (26). Obviously there are 'good' normal deformations for which the WNA is an excellent approximation (P1 and W8 in Fig. 4, for example), and there are 'bad' normal deformations for which the WNA is not a very good approximation (FR in Fig. 4, and the normal component in Fig. 14b). In this section we present numerical evidence that verifies the theoretical results of the previous section, and investigate how 'bad' a normal deformation has to be for them to break down.

From what we have claimed it follows that if $D_1(\mathbf{s})$ and $D_2(\mathbf{s})$ are orthogonal normal deformations, then $\nu_{1+2} = \nu_1 + \nu_2$. We could as well write

$$\tilde{C}_{1+2}(\omega) \approx \tilde{C}_1(\omega) + \tilde{C}_2(\omega)$$

$$\text{if } 1\text{=normal, } 2\text{=normal, and } 1 \perp 2 \qquad (29)$$

because by assumption the three correlation functions are approximately flat. We demonstrate this addition rule in the case of two 'good' deformations which are orthogonal in Fig. 9. We found that small 'pistons' (P2 is significant on only $\sim 1/50$ of the perimeter) were needed to achieve addition of the accuracy (a few %) shown. However, the restriction on the 'wiggle' type of deformation was somewhat more lenient (WG is ~ 5 times wider than P2 yet obeys the WNA better than P2 does).

In general we observe that the quality of the addition rule is limited by the deviation from the WNA of the *better* of the two deformations. In Fig. 10 we see that if both $D_1(\mathbf{s})$ and $D_2(\mathbf{s})$ are bad, then also the addition rule (29) becomes quite bad. Fig. 11 shows that the addition rule (29) is reasonably well satisfied also if *either* $D_1(\mathbf{s})$ or $D_2(\mathbf{s})$ is a 'good' normal deformation. We have chosen $D_1(\mathbf{s})$ as WG (good), and $D_2(\mathbf{s})$ as SX which is almost completely dominated by the special x-translation deformation. The addition rule (29) is obeyed at all ω. This proves that our assertions
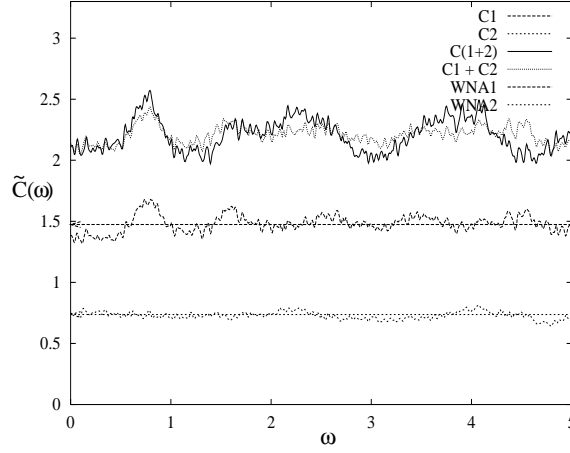
Figure 9. Addition of two 'good' normal deformations (1=P2, 2=WG). The two are orthogonal in the sense of (26). That they are 'good' can be seen by their good agreement with their WNA results (horizontal arrows). The power spectrum of the sum agrees well with the sum of the power spectra.

Eq.(25) about the vanishing of $C_{1,2}^{\text{non-self}}(\tau)$ is indeed correct. It holds here as a non-trivial statement ($D_2(\mathbf{s})$ is general and 'bad').

Finally, we consider the case where $D_1(\mathbf{s})$ is general and $D_2(\mathbf{s})$ is special. This is illustrated in Fig. 12. The addition rule (29) becomes exact in the limit of small frequency corresponding to the vanishing of $\tilde{C}_{1,2}(\omega \to 0)$ as implied by Eq.(24). In particular this implies that $\nu_{1+2} = \nu_1$. Note that there is *no* condition on the orthogonality of $D_1(\mathbf{s})$ and $D_2(\mathbf{s})$). This will be the key to for improving over the WNA, which we are going to discuss in the next section.

In drawing the above conclusions it is important to note that symmetry effects can play a deceptive role if the cavity shape has symmetry (our example Fig. 1 is in the C_{2v} symmetry group). In Fig. 13 we demonstrate that the addition rule (29) is very accurately satisfied at *all* ω if $D_1(\mathbf{s})$ and $D_2(\mathbf{s})$ belong to different symmetry classes of the cavity. Orthogonality of $D_1(\mathbf{s})$ and $D_2(\mathbf{s})$ is *not* sufficient to explain this perfect linearity of addition of $\tilde{C}_{\text{E}}(\omega)$. Rather, it follows from the symmetry of the kernel $\gamma_{\text{E}}(\mathbf{s}_1, \mathbf{s}_2)$ of Eq.(12). The cross-terms in (12) rigorously vanish when such deformations are added. The consequence is that in order to demonstrate the assertions of this and of the previous section, we had to choose deformations of the *same* symmetry class, or which break all symmetries of the cavity.

10. Beyond the WNA

It is possible now to consider the case of general deformation, and to go beyond the WNA. Given a general deformation $D(\mathbf{s})$ we should project out (subtract) all the special components, leaving the normal component, and only then apply the WNA. In Fig. 14 we demonstrate this decomposition for the deformation (CO + W16) and the deformation SX.

The special deformations constitute a linear space which is spanned by the basis functions: one dilation, d translations, and $d(d-1)/2$ rotations. (For d=2 they are
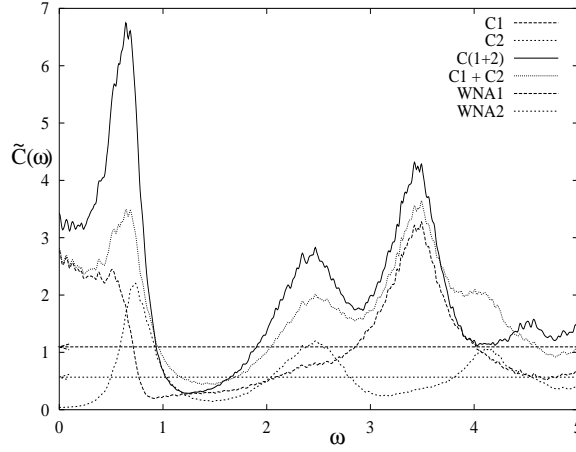
Figure 10. Addition of two 'bad' normal deformations (1=FR, 2=SX). The two are orthogonal in the sense of (26). That they are 'bad' is shown by a lack of agreement with their WNAs. The power spectrum of the sum is badly approximated by the sum of the power spectra (non-linear addition).
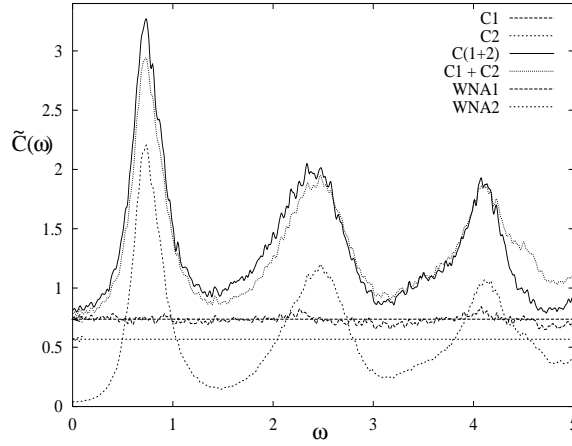

Figure 11. Addition of a 'good' normal deformation (1=WG) to a general deformation (2=SX). The two are orthogonal in the sense of (26). The power spectrum of the sum agrees well with the sum of the power spectra.

listed in Table II). For a general cavity shape these basis functions are not orthogonal. However, because they are linearly independent, we can use standard linear algebra to build an orthonormal basis $\{D_i(\mathbf{s})\}$ of special deformations. The special ($\parallel$) and the normal ($\perp$) components of any given deformation $D(\mathbf{s})$ are therefore

$$D_{\parallel}(\mathbf{s}) = \sum_i \alpha_i D_i(\mathbf{s})$$
$$D_{\perp}(\mathbf{s}) = D(\mathbf{s}) - D_{\parallel}(\mathbf{s}) \tag{30}$$

where the coefficients are

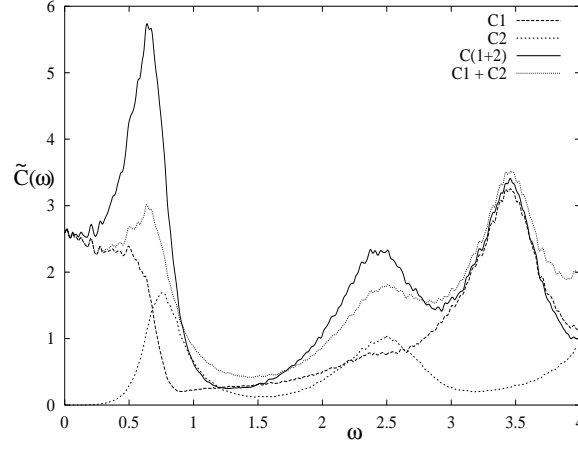$$\alpha_i = \oint D(\mathbf{s})D_i(\mathbf{s})\,d\mathbf{s}. \tag{31}$$

Figure 12. Addition of a general deformation (1=FR) to 'special' deformation (2=TX). The power spectrum of the sum coincides with the sum of the power spectra in the limit $\omega \to 0$, as implied by Eq.(27).
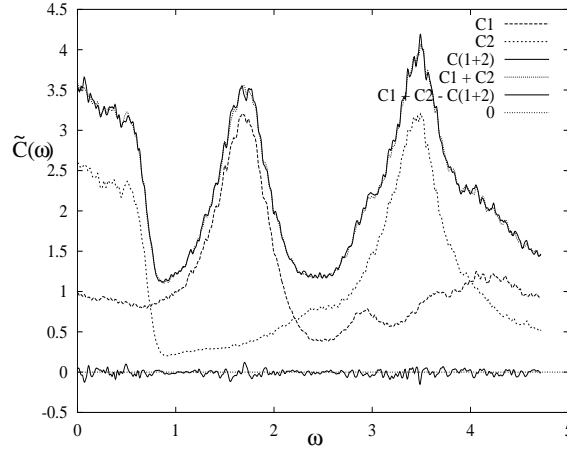

Figure 13. Addition of two 'bad' general deformations which come from different symmetry classes of the cavity (1=W2, 2=FR). The two must also be orthogonal, by symmetry. The deviation from linear addition (solid line varying about zero) vanishes at all ω.

The improved approximation for ν applies the WNA only to the normal component, giving

$$\nu_{\mathrm{E}} \approx 2m^2 v_{\mathrm{E}}^3 \langle |\cos\theta|^3 \rangle \frac{1}{V} \oint d\mathbf{s}[D_\perp(\mathbf{s})]^2 \qquad (32)$$

which we name the IFIF (Improved Fluctuations Intensity Formula). In the particular case of d=3, substitution of this result into the microcanonical FD relation gives an 'improved wall formula' consisting of the replacement of $D(\mathbf{s})$ by $D_\perp(\mathbf{s})$ in Eq. (5).

In Fig. 14 we use the IFIF to estimate ν for two examples. The first is a deformation (CO + W16) whose normal component is 'good', due its oscillatory nature. The deviation from a flat white power spectrum is $\sim 20\%$ for the normal
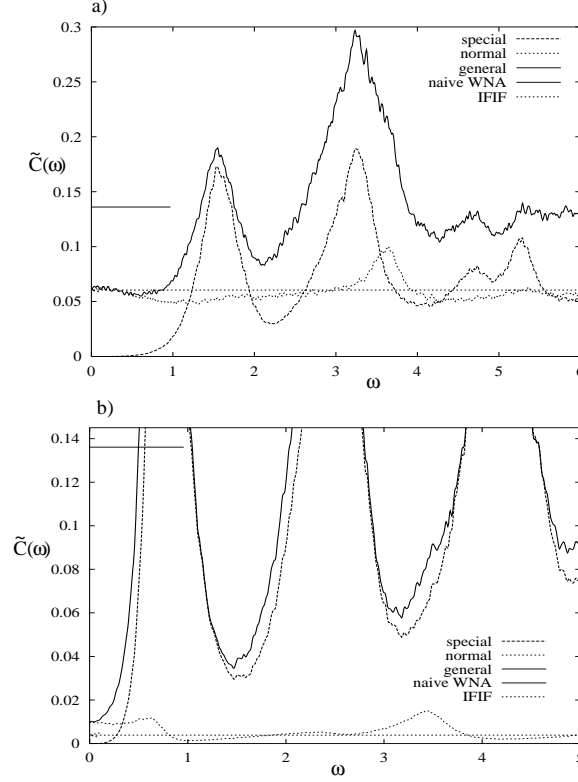
Figure 14. Decomposition of general deformations $D(s)$ into orthogonal 'normal' and 'special' components. The general deformation is CO + W16 in subfigure (a), and SX in subfigure (b). The naive WNA Eq.(14) is indicated by short solid line. The improved (IFIF) result Eq.(32) is indicated by long dashed arrow.

component. The IFIF result Eq.(32) is accurate to a few percent. It is a much better estimate of the actual ν compared with the naive WNA Eq.(14) which overestimates the correct value by a factor of 2.2. In the second example the deformation is SX. The resulting normal component is 'bad'. Its power spectrum fluctuates by a factor of about 10 in the ω range shown. Consequently the IFIF is limited in its accuracy, and the correct value for ν is underestimated by a factor of 2.5. However, it is still a great improvement over the naive result Eq.(14). In this second example we can extract another prediction about $\tilde{C}_{\mathrm{E}}(\omega)$. The special component is a factor ~ 10 larger than the normal component. Therefore the ω^2 behavior at small ω is almost entirely due to the 'rotation' component. The prefactor of the ω^2 behavior need only be found once for each billiard shape (see Section 6). This saves computation and gives an extra information about the dissipation rate at finite driving frequency.

A few concluding remarks regarding the history of the wall formula are in order. It has been known since its inception that the naive wall formula gives unphysical answers in the case of *constant-velocity* translations and rotations. This was first regarded as a kinetic gas 'drift' effect [2]. It should be noted that the recipe presented in [2], namely to subtract this drift component, is equivalent in practice to the recipe (30) that we have presented here, *provided we ignore dilations*. It is also important
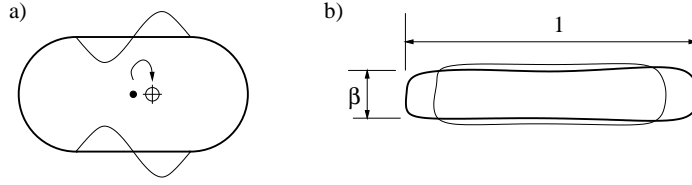
Figure 15. **a**) A deformation of the stadium which moves the 'center of mass' (centroid) of the cavity to the right (from the dot to the crosshairs symbol). This deformation is orthogonal (in the sense of (26)) to all special deformations, in particular, all translations. **b**) An example volume-preserving deformation of an elongated approximately-rectangular cavity ($\beta \ll 1$) which nevertheless has a large overlap with dilation. It can be shown that this results in an IFIF estimate of $\approx 4\beta$ times that of the naive WNA. In both diagrams the undeformed shape is shown as a heavy line, the deformed one as a thin line.

to realize that the argumentation in [2] for this subtraction appears to be ad hoc, being based on a 'least-structured drift pattern' reasoning. A stated condition on this subtraction was that the resulting deformation preserve the location of the 'center of mass' (centroid) of the cavity, for reasons particular to the nuclear application [2]. This condition seems to have become standard practice in numerical tests of the wall formula [10, 27, 28, 29]. However, as the system in Fig. 15a illustrates, this condition is generally *not* equivalent to the above subtraction of translation and rotation components [30]. This seems to invalidate the theorem presented in Section 7.1 of [2]. Where the flaw in their reasoning lies we are not sure.

The consideration of the special nature of dilations is absent from the literature. Even if we restrict ourselves to volume-preserving deformations (the case for the nuclear application), then deformations of certain cavities can be found for which the dilation correction is significant; we illustrate this in Fig. 15b. This correction can only be large if the cavity has a large variation in radius (*i.e.* is highly non-spherical). We suggest this as a possible reason why major discrepancies due to dilation have not emerged in the numerical tests of the wall formula until now. Such tests have generally been of shapes close to a 3D sphere [2, 10, 27, 28, 29].

Hence we believe that the recipe we have presented, along with the associated theory and in conjunction with the particular power-law dependences, is a significant step in the treatment of one-body dissipation.

Acknowledgments

Appendix A. Linear response theory of dissipation

Given a parametric Hamiltonian $H(Q, P; x(t))$, and given initial conditions, one defines the energy $\mathcal{E}(t) = H(Q(t), P(t); x(t))$ and the fluctuating quantity $\mathcal{F}(t) = -\partial\mathcal{H}/\partial x(Q(t), P(t); x(t))$. With no approximation we have

$$\mathcal{E}(t) - \mathcal{E}(0) = \int_0^t \mathcal{F}(t')\dot{x}(t')dt'. \tag{A.1}$$

Using the same steps as in [8] one obtains the following result for the variance of the energy spreading:

$$\delta E(t)^2 = \int_0^t \int_0^t C_{\mathrm{E}}(t'' - t')F(t'' - t')dt'dt'' \tag{A.2}$$

where $C_{\mathrm{E}}(\tau)$ is defined by Eq.(11). Microcanonical averaging has been taken over the initial conditions. The function $F(\tau) = \langle\dot{x}(t)\dot{x}(t + \tau)\rangle$ is the velocity-velocity correlation of the driving. For periodic driving $x(t) = A\sin(\Omega t + \text{phase})$ it is formally convenient to average over the initial phase and one obtains $F(\tau) = \frac{1}{2}(A\Omega)^2\cos(\Omega\tau)$.

For a chaotic system $C_{\mathrm{E}}(\tau)$ is characterized by some correlation time τ_{cl}. For $t \gg \tau_{\mathrm{cl}}$ one obtains diffusive spreading $\delta E(t)^2 = 2D_{\mathrm{E}}t$ where the diffusion rate is

$$D_{\mathrm{E}} = \frac{1}{2}\tilde{C}_{\mathrm{E}}(\Omega) \times \frac{1}{2}(A\Omega)^2 \tag{A.3}$$

which for small frequencies goes to $D_{\mathrm{E}} = \frac{1}{2}\nu_{\mathrm{E}}V^2$, where $\nu_{\mathrm{E}} \equiv \tilde{C}(0)$ as defined in the Introduction. The picture to keep in mind is that of the fluctuating $\mathcal{F}(t)$ causing a *random walk* in energy space via Eq.(A.1) for times $t \gg \tau_{\mathrm{cl}}$. As explained in [4, 5, 8] the resulting diffusion in energy space implies systematic *growth* of the average energy. It is important to realise that this growth happens even if the random walk is locally unbiased: such is the case when changing the parameter x preserves the volume of a given energy-shell in phase-space. (For a deforming billiard system this corresponds to preservation of the billiard volume). The rate of energy growth is related to the diffusion as follows:

$$\frac{d}{dt}\langle\mathcal{H}\rangle = -\int_0^\infty dE\; g(E)\; D_{\mathrm{E}}\; \frac{\partial}{\partial E}\left(\frac{\rho(E)}{g(E)}\right) \tag{A.4}$$

where $\rho(E)$ is the energy distribution of the particles, and $g(E)$ is the one-particle density of states. The growth is therefore an effect of the E-dependence of both the diffusion rate and the density of states.

The rate of dissipation can be written as in Eq.(1) or as $d\langle\mathcal{H}\rangle/dt = \mu V^2$ in the small frequency limit. Combining this with Eq.(A.4) implies a relation between the dissipation coefficient μ and the function $\tilde{C}_{\mathrm{E}}(\omega)$. The most familiar version of this FD relation is obtained for small frequency under the assumption of a canonical distribution $\rho(E) \propto g(E)\exp(-E/(k_B T))$, leading to

$$\mu = \frac{1}{2k_B T}\nu \tag{A.5}$$

where ν should be calculated for a canonical distribution. This result should be multiplied by the number of non-interacting classical particles.

The use of Eq.(A.4) can be justified also for non-interacting fermions [31]. This is because the effect of Pauli exclusion principle cancels out (in analogy with Boltzmann

picture with elastic scattering). Substituting $\rho(E) = g(E)f(E-E_{\mathrm{F}})$, where $f(E-E_{\mathrm{F}})$ is the Fermi occupation function, one obtains

$$\mu = \frac{1}{2}g(E_{\mathrm{F}})\nu_{\mathrm{F}} \qquad\qquad (A.6)$$

where ν_{F} should be calculated at the Fermi energy.

Finally, the microcanonical version of the FD relation is

$$\mu_{\mathrm{E}} = \frac{1}{2}\frac{1}{g(E)}\frac{\partial}{\partial E}(g(E)\nu_{\mathrm{E}}) \qquad\qquad (A.7)$$

The subscript E indicates that both ν_{E} and μ_{E} are evaluated locally around some energy E.

Appendix B. Cross correlations I

In this Appendix we introduce two proofs of Eq.(24). The first is a formal argument, while the second is a more physically appealing argument. The formal argument is as follows: Eq.(12) is an exact result which can be written using obvious abstract matrix notation as $\nu = D\gamma_{\mathrm{E}}D$. Let $D = D_1 + D_2$. If D_2 is a special deformation then by definition $D_2\gamma_{\mathrm{E}}D_2 = 0$. But this can be true only if D_2 belongs to the kernel (nullspace) of the matrix γ_{E}, hence we have $\gamma_{\mathrm{E}}D_2 = 0$. Therefore we have also $D_1\gamma_{\mathrm{E}}D_2 = 0$ for any D_1, which is precisely the statement of Eq.(24).

Now we present the alternative physically appealing argument. Consider two noisy signals $\mathcal{F}(t)$ and $\mathcal{G}(t)$. We assume that $\langle\mathcal{F}(t)\rangle = \langle\mathcal{G}(t)\rangle = 0$. The angular brackets stand for an average over realizations. The auto-correlations of $\mathcal{F}(t)$ and $\mathcal{G}(t)$ are described by functions $C_{\mathrm{F}}(\tau)$ and $C_{\mathrm{G}}(\tau)$ respectively. We assume that both auto-correlation functions are short-range, meaning no power-law tails (this corresponds to the hard chaos assumption of this paper), and that they are negligible beyond a time τ_{c}. We call a signal 'special' if the algebraic area under its auto-correlation is zero. The cross-correlation function is defined as

$$C_{\mathrm{F,G}}(\tau) \equiv \langle\mathcal{F}(t')\mathcal{G}(t'')\rangle, \qquad \tau \equiv t' - t''. \qquad\qquad (B.1)$$

We assume stationary processes so that the cross-correlation function depends only on the time difference τ. We also symmetrize this function if it does not have $\tau \mapsto -\tau$ symmetry. We assume that $C_{\mathrm{F,G}}(\tau)$ is short-range, meaning that it becomes negligibly small for $|\tau| > \tau_{\mathrm{c}}$. We would like to prove that if either $\mathcal{F}(t)$ or $\mathcal{G}(t)$ is special then the algebraic area under the cross-correlation function equals zero.

Consider the case where $\mathcal{F}(t)$ is general while $\mathcal{G}(t)$ is special. The integral of $C_{\mathrm{F}}(\tau)$ will be denoted by ν. Define the processes

$$X(t) = \int_0^t \mathcal{F}(t')dt' \qquad\qquad (B.2)$$

$$Y(t) = \int_0^t \mathcal{G}(t'')dt''. \qquad\qquad (B.3)$$

From our assumptions it follows, disregarding a transient, that for $t \gg \tau_{\mathrm{c}}$ we have diffusive growth $\langle X(t)^2\rangle \approx \nu t$. However since $Y(t)$ is a stationary process [32], $\langle Y(t)^2\rangle \approx \text{const}$. Therefore for a typical realization we have $|X(t)| \leq \text{const} \times \sqrt{\nu t}$ and $|Y(t)| \leq \text{const}$. Consequently, without making any claims on the independence of

$X(t)$ and $Y(t)$, we get that $\langle X(t)Y(t)\rangle$ cannot grow faster than const $\times \sqrt{\nu t}$. Using the definitions (B.2), (B.3) and (B.1) we can write

$$\int_{-\infty}^{\infty} C_{\text{F,G}}(\tau)d\tau = \frac{\langle X(t)Y(t)\rangle}{t} \approx \frac{\text{const}}{\sqrt{t}} \to 0 \tag{B.4}$$

where the limit $t \to \infty$ is taken. Thus we have proved our assertion.

Appendix C. Cross correlations II

In this section we further discuss some features of the cross-correlation function. For the purpose of presentation we we would like to view the time as an integer variable $t = 1, 2, 3....$ One may think of each instant of time as corresponding to a bounce.

Let us assume that we have functions $f(s)$ and $g(s)$, and a time-sequence $(s_1, s_2, s_3, ...)$. This gives two stochastic-like processes $(\mathcal{F}_1, \mathcal{F}_2, \mathcal{F}_3, ...)$ and $(\mathcal{G}_1, \mathcal{G}_2, \mathcal{G}_3, ...)$. The cross correlation of these two processes is defined as follows:

$$C_{\text{F,G}}(i - j) = \langle \mathcal{F}_i \mathcal{G}_j \rangle = \langle f(s_i)g(s_j) \rangle \tag{C.1}$$

It is implicit in this definition that we assume that the processes are stationary, so the result depends only on the difference $\tau = (i - j)$. The angular brackets stand for an average over realizations of s-sequences.

If the sequences are ergodic on the s domain, then it follows that

$$\langle \mathcal{F} \rangle \quad = \int f(s)ds$$

$$\langle \mathcal{G} \rangle \quad = \int g(s)ds$$

$$C_{\text{F,G}}(0) = \int f(s)g(s)ds \tag{C.2}$$

The $\tau \neq 0$ cross-correlations requires information beyond mere ergodicity. In case that the s sequence is completely uncorrelated in time we can factorized the averaging and we get $C_{\text{F,G}}(\tau \neq 0) = \langle \mathcal{F} \rangle \times \langle \mathcal{G} \rangle$. If $\langle \mathcal{F} \rangle = 0$ then

$$C_{\text{F,G}}(\tau \neq 0) = 0 \tag{C.3}$$

irrespective of $\langle \mathcal{G} \rangle$.

However, we would like to define circumstances in which Eq.(C.3) is valid, even if the s sequence is *not* uncorrelated. In such case either the $\mathcal{F}$ or the $\mathcal{G}$ may possess time correlations. (Such is the case if $\mathcal{G}$ is 'special'). So let us consider the case where the $\mathcal{F}$ sequence *looks random*, while assuming nothing about the $\mathcal{G}$ sequence. By the phrase 'looks random' we mean that the conditional probability satisfies

$$\text{Prob}(\mathcal{F}_i|s_j) = \text{Prob}(\mathcal{F}_i) \qquad \text{for any } i \neq j \tag{C.4}$$

Eq. (C.3) straightforwardly follows provided $\langle \mathcal{F} \rangle = 0$, irrespective of the $g(s)$ involved. Given $f(s)$, the goodness of assumption (C.4) can be actually tested. However, it is not convenient to consider (C.4) as a practical definition of a 'normal' deformation.

References

[1] For review and references see S. Fishman in *Proceedings of the International School of Physics "Enrico Fermi", Course CXIX*, Ed. G. Casati, I. Guarneri and U. Smilansky (North Holland 1993).

[2] J. Blocki, Y. Boneh, J.R. Nix, J. Randrup, M. Robel, A.J. Sierk and W.J. Swiatecki, Ann. Phys. **113**, 330 (1978).

[3] S.E. Koonin, R.L. Hatch and J. Randrup, Nucl. Phys. A **283**, 87 (1977); S.E. Koonin and J. Randrup, Nucl. Phys. A **289**, 475 (1977).

[4] C. Jarzynski, Phys. Rev. A **46**, 7498 (1992).

[5] C. Jarzynski, Phys. Rev. E **48**, 4340 (1993).

[6] E.J. Austin and M. Wilkinson, J. Phys: Condens. Matter **5**, 8461 (1993). See also **6**, 4153 (1994).

[7] D. Cohen in *Proceedings of the International School of Physics "Enrico Fermi" Course CXLIII*, Ed. G. Casati, I. Guarneri and U. Smilansky (IOS Press, Amsterdam 2000).

[8] D. Cohen, Annals of Physics **283**, 175-231 (2000).

[9] Consider the case of a deformation which involves only a small piece of the boundary. Typically, the time between collisions with the deforming piece is $\tau_{\rm col}$. However, correlations are dominated by the rare events when the time between collisions is $\sim \tau_{\rm bl}$.

[10] S. Pal and T. Mukhopadhyay, Phys. Rev. C **54**, 1333-1340 (1996); T. Mukhopadhyay and S. Pal, Phys. Rev. C **56**, 296-301 (1997).

[11] L. A. Bunimovich, Sov. Phys. JETP **62**, 842 (1985).

[12] M. Wojtkowski, Commun. Math. Phys. **105**, 391-414 (1986).

[13] D. Cohen, Phys. Rev. Lett. **82**, 4951 (1999).

[14] D. Cohen and T. Kottos, cond-mat/0004022, Phys. Rev. Lett. (2000, in press).

[15] The cross-product form used here for $\mathbf{D}$ and $\mathcal{G}(t)$ is strictly valid in 2D and 3D only. For $d > 3$ the higher-dimensional generalization of a general rotation should be used.

[16] A. H. Barnett, D. Cohen, and E. J. Heller, Phys. Rev. Lett. **85**, 1412 (2000).

[17] D. Cohen and T. Kottos, nlin.CD/0001026, submitted to *Phys. Rev. E*.

[18] D. Cohen, A. H. Barnett, and E.J. Heller, nlin.CD/0008040, submitted to *Phys. Rev. E*.

[19] E. Vergini and M. Saraceno, Phys. Rev. E, **52**, 2204 (1995).

[20] A. H. Barnett, Ph. D. thesis, Harvard University, 2000.

[21] E. Vergini, Ph. D. thesis, Universidad de Buenos Aires, 1995.

[22] S. M. Hammel, J. A. Yorke, and C. Grebogi, J. Complexity **3**, 136 (1987); C. Grebogi, S. M. Hammel, J. A. Yorke, and T. Sauer, Phys. Rev. Lett. **65**, 1527 (1990).

[23] B. Friedman and R. F. Martin, Jr., Phys. Lett. **105A**, 23 (1984).

[24] P. Dahlqvist and R. Artuso, Phys. Lett. **219A**, 212 (1996).

[25] Time of crossover to algebraic decay is discussed in P. Dahlqvist, Phys. Rev. E **60**, 6639 (1999).

[26] R. Brown, E. Ott, and C. Grebogi, J. Stat. Phys. **49**, 511 (1987).

[27] J. Blocki, F. Brut, and W. J. Swiatecki, Nucl. Phys. A **554**, 107 (1993).

[28] J. Blocki, Y.-J. Shi, and W. J. Swiatecki, Nucl. Phys. A **554**, 387 (1993).

[29] J. Blocki, J. Skalski, and W. J. Swiatecki, Nucl. Phys. A **594**, 137 (1995).

[30] The condition that a deformation $D(\mathbf{s})$ not move the 'center of mass' (centroid of the cavity volume) is $\oint D(\mathbf{s})\mathbf{r}(\mathbf{s})\,d\mathbf{s} = \mathbf{0}$. This is in general different from the condition for having zero overlap with translations, namely $\oint D(\mathbf{s})\hat{\mathbf{n}}(\mathbf{s})\,d\mathbf{s} = \mathbf{0}$.

[31] M. Wilkinson, J. Phys. A **23**, 3603 (1990).

[32] C. W. Gardiner, *Handbook of Stochastic Methods* (Springer-Verlag, 1983).